



On the spectral properties and excitation dynamics of long-wavelength chlorophylls in higher-plant photosystem I

Parveen Akhtar, Petar H. Lambrev*

Biological Research Centre, Szeged, Temesvári krt. 62, Szeged 6726, Hungary



ARTICLE INFO

Keywords:

Energy transfer
Excitation trapping
Light harvesting
Photosynthesis
Red chlorophylls
Time-resolved fluorescence

ABSTRACT

In higher-plant Photosystem I (PSI), the majority of “red” chlorophylls (absorbing at longer wavelengths than the reaction centre P_{700}) are located in the peripheral antenna, but contradicting reports are given about red forms in the core complex. Here we attempt to clarify the spectroscopic characteristics and quantify the red forms in the PSI core complex, which have profound implication on understanding the energy transfer and charge separation dynamics. To this end we compare the steady-state absorption and fluorescence spectra and picosecond time-resolved fluorescence kinetics of isolated PSI core complex and PSI-LHCI supercomplex from *Pisum sativum* recorded at 77 K. Gaussian decomposition of the absorption spectra revealed a broad band at 705 nm in the core complex with an oscillator strength of three chlorophylls. Additional absorption at 703 nm and 711 nm in PSI-LHCI indicated up to five red chlorophylls in the peripheral antenna. Analysis of fluorescence emission spectra resolved states emitting at 705, 715 and 722 nm in the core and additional states around 705–710 nm and 733 nm in PSI-LHCI. The red states compete with P_{700} in trapping excitations in the bulk antenna, which occurs on a timescale of ~ 20 ps. The three red forms in the core have distinct decay kinetics, probably in part determined by the rate of quenching by the oxidized P_{700} . These results affirm that the red chlorophylls in the core complex must not be neglected when interpreting kinetic experimental results of PSI.

1. Introduction

Photosystem I (PSI) has structure and composition highly conserved among all oxygen-evolving photosynthetic organisms [1–3]. It harbors ~ 98 chlorophylls *a* (Chl *a*) and ~ 22 carotenoids, coordinated by the two largest subunits PsaA and PsaB. Together with the cofactors of the reaction centre (RC), they form a fused core antenna – RC assembly. In green algae and higher plants, the light-harvesting capacity of PSI is enhanced by the attachment of several subunits of light-harvesting complex I (LHCI) to form a PSI-LHCI supercomplex [4,5], a PSI-FCPI supercomplex exists in diatoms [6]. The LHCI complexes of higher plants are present in single copies per PSI and organized as two heterodimers, Lhca1/4 and Lhca2/3 [7], located on one side of the core complex in a half-moon shape; taken together, they bind ~ 60 Chl *a* + *b* and ~ 13 carotenoids [4].

PSI of almost all organisms contains long-wavelength Chl forms, dubbed “red” Chls, absorbing light at wavelengths longer than the absorption of the RC Chls P_{700} [8], broadening the absorption spectral range. The red forms are characterized by long-wavelength emission, large Stokes shift, large homogeneous and inhomogeneous broadening and unusually high electron-phonon coupling – properties attributed to

the mixing of excitonic and charge-transfer states [9–13]. The number of the red Chl forms is species-dependent and their emission maxima vary between different organisms in the range of 700 to 760 nm [14,15]. The majority of the low-energy Chl forms in plants have been shown to reside on LHCI [16–20]. However, several authors have reported a range of values regarding the number of red Chls, their energies and distribution in the core complex and LHCI [9,14,17]. Some have hypothesized that red states at the interface between the core and LHCI maybe lost during their biochemical separation [5].

Although red Chls account for only a small fraction (3–10%) of the total absorption cross-section [21], they have sizeable impact on the dynamics of excitation energy transfer (EET) and trapping, as the excitations must be transferred energetically uphill to the RC [22,23]. The excitation dynamics of PSI has been investigated by many workers. Pioneering picosecond fluorescence studies in the 1970s revealed that PSI fluorescence decays in 80 ps or less at room temperature [24,25] but the lifetimes are drastically slower at cryogenic temperatures because of trapping of excitations on long-wavelength Chls [22,26]. Despite the abundance of time-resolved spectroscopy data, the EET and trapping kinetics are still under debate [3,21]. In most organisms, photochemical trapping of excitations in the bulk antenna occurs on a

* Corresponding author.

E-mail address: lambrev.petar@brc.hu (P.H. Lambrev).

<https://doi.org/10.1016/j.bbambio.2020.148274>

Received 26 May 2020; Received in revised form 13 July 2020; Accepted 19 July 2020

Available online 23 July 2020

0005-2728/ © 2020 The Author(s). Published by Elsevier B.V. This is an open access article under the CC BY-NC-ND license

(<http://creativecommons.org/licenses/by-nc-nd/4.0/>).

timescale of about 20 ps [14,27–30]. This has been ascribed to reflect predominantly electron transfer in the RC, i.e. trap-limited kinetics [28,31,32] or EET to P_{700} , i.e. transfer-to-trap-limited [14,33–37]. Slower components are observed in PSI with higher abundance of red Chls or more red-shifted forms [14], and in PSI–LHCI supercomplexes [23,29,30,38–40].

A fast process of energy equilibration, typically on a timescale of 2–4 ps at room temperature [14,34,41–47] and 4–6 ps at cryogenic temperature [44,48,49], has been assigned to EET from the bulk antenna Chls to the red forms. The spectral changes on this timescale could also be interpreted as arising from excitation of the RC pigments followed by charge separation [28,31,32,50]. In recent investigations of PSI from higher plants, the bleaching of states absorbing around 700 nm observed on a 2–4 ps timescale, was attributed to the RC pigments [30,51]. One of the reasons for such assignment was that the majority of red Chls in plant PSI are located in the peripheral antenna, whereas the species in question was observed in the core.

As the red Chls can significantly affect the PSI kinetics, their stoichiometry, energetic properties, and subunit distribution must be taken into account in any informed model. Therefore, in this work we revisited the red Chl content of the PSI core complex and the intact PSI–LHCI from *Pisum sativum* by comparing their steady-state absorption and fluorescence emission spectra recorded at 77 K. We were able to resolve multiple spectral forms emitting in the far-red region belonging to both the core and peripheral antenna. There are very few low-temperature time-resolved spectroscopy studies on the dynamics of plant PSI [38,52] and none report the detailed kinetics of the isolated core. We recorded the picosecond fluorescence decays of PSI–LHCI and the isolated core complex at 77 K, allowing us to kinetically resolve the different red Chl forms and propose a model for the kinetics of excitation energy equilibration between them.

2. Materials and methods

2.1. Sample preparation

PSI-enriched stromal membrane vesicles isolated from 14-days-old greenhouse grown pea (*Pisum sativum*) according to the protocols of Peters et al. [53] were used as a starting material for PSI–LHCI supercomplexes. The preparations having Chl *a/b* ratio of 9–10 were further purified by solubilization with dodecyl- β -maltoide (β -DDM, Cube Biotech, Germany) and sucrose density gradient ultracentrifugation as described in Akhtar et al. [54]. PSI core complexes were obtained by further treatment with Zwittergent-16 using the previously described protocol [30]. The Chl content of the preparations was determined from acetone extracts using the coefficients of Porra [55]. PSI–LHCI preparations had Chl *a/b* ratio of 12.8 (Supplementary Table S1), which closely matches the pea crystal structure of Qin et al. [4]. The purity of the PSI core preparations was evaluated by their Chl *b* content (< 0.4%) and Lhca1 content, by immunoblotting (Supplementary Fig. S1). From the analysis, we estimate a stoichiometry ratio of ≤ 0.2 LHCI subunits per PSI core (2% of the total Chl *a* content).

2.2. Absorption spectroscopy

Absorption spectra at 77 K were recorded between 350 and 750 nm with a J-815 (Jasco, Japan) spectrometer, with spectral bandwidth of 1 nm. The samples were diluted to absorbance of one at the red Chl maximum in buffer medium containing 60% (v/v) glycerol, 20 mM tricine and 0.03% β -DDM. The solutions were placed into a demountable quartz cuvette of 1-mm optical path length and cooled to 77 K in an optical cryostat (Optistat DN, Oxford Instruments, UK).

2.3. Steady-state fluorescence spectroscopy

Fluorescence emission spectra at 77 K were recorded with a

Fluorolog 3 double-monochromator spectrofluorometer (Horiba Jobin-Yvon, USA). The sample suspension (40–50 μ l) with absorbance of 0.5 per cm was deposited on Whatman glass fiber discs. The filters were then immersed in liquid nitrogen and transferred to a Dewar vessel filled with liquid nitrogen that was placed into the measurement chamber of the spectrofluorometer. Emission spectra from 600 to 800 nm were recorded with excitation wavelengths of 436 nm and 470 nm and excitation/emission bandwidth of 3 nm. The measurements were performed with 1 nm increment and 1 s integration time.

2.4. Time-resolved fluorescence

Fluorescence decays were recorded by time-correlated single-photon counting (TCSPC) using an instrument described in Akhtar et al. [54] at emission wavelengths 670–760 nm with 5-nm step. The samples were diluted to an absorbance of 0.03 (at room temperature) in the same buffer as for absorption measurements. The excitation pulses from a Fianium WhiteLase Micro (NKT Photonics, UK) supercontinuum laser at 20 MHz repetition rate were centred at 440 nm. The energy per pulse was approximately 10^{-13} J, focused on a spot of ~ 200 μ m diameter, corresponding to $7 \cdot 10^8$ photons/cm². Assuming a total Chl absorption cross-section of the PSI core equal to $98.5 \cdot 10^{-16}$ cm², this is equivalent to ~ 0.7 excitations/ms. The total instrument response (IRF) width was 40 ps, measured using 1% Ludox as scattering solution. Similar results were obtained using 632 nm excitation pulses.

2.5. Data analysis

All data analysis was performed in MATLAB. The fluorescence decays collected at different wavelengths were subjected to global multiexponential lifetime analysis routine with IRF deconvolution to obtain lifetimes and decay-associated emission spectra (DAES).

3. Results

3.1. Steady-state absorption and emission spectra

3.1.1. Spectral decomposition of the absorption spectra

The absorption spectra of isolated PSI core complexes and intact PSI–LHCI plotted in Fig. 1 show that the supercomplex absorbs more light at wavelengths above 700 nm than the core complex, in accordance with all previous reports on plant PSI [9,17]. For a more quantitative description, we decomposed the spectra in the red wavelength region into components with a skew-gaussian shape in the frequency domain. The asymmetric lineshapes more closely resemble Chl absorption bands and resulted in a markedly improved fit [16,56]. Nevertheless, here we do not delve into the physical meaning of all spectral components but focus on the red Chls only, which we define as those that absorb at wavelengths longer than 700 nm (i.e. with energies below the RC). The red-most component of the core complex spectrum is centred at 705 nm and has width (FWHM) of 23 nm (Supplementary Table S2). The band's integrated area is 2.4% of the total Q-band absorption. However, if the two shortest-wavelength bands, at 615 and 634 nm, are not counted, as they likely originate from higher vibronic and electronic states (Q_x), the 705-nm band accounts for 3.3% of the total absorption. Hence, the band represents red antenna states in the core complex with an oscillator strength of about three Chls – assuming 98 Chls in total. Note that the next band, at 698 nm, amounting to two Chls, can be attributed to the RC. We should stress that we refer to three red Chls in the core, based on the relative oscillator strength, but the actual number of Chl molecules contributing to the molecular states is likely larger.

Applying the same analysis to the 77 K absorption spectrum of the intact PSI–LHCI supercomplex, we obtained six components peaking above 670 nm, of which the two red-most have maxima at 703 nm and 712 nm. The integrated area of the two far-red bands is 7% of the total

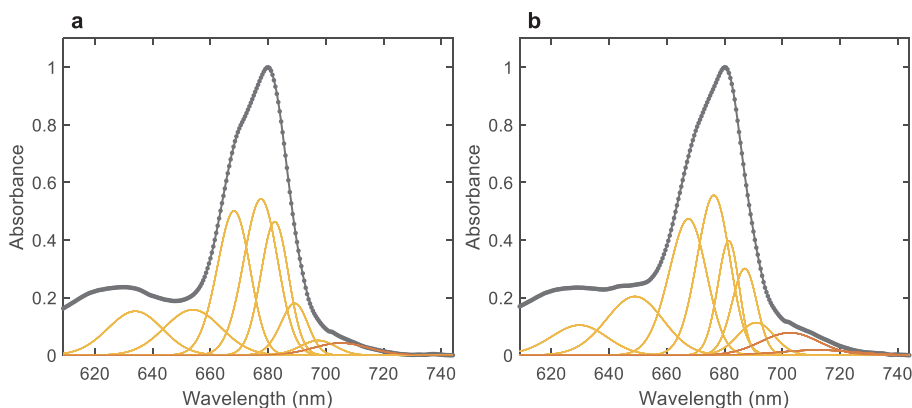


Fig. 1. Gaussian decomposition analysis of the Chl Q_y absorption spectra of PSI at 77 K. (a) PSI core complex; (b) PSI-LHCI supercomplex. Gray symbols indicate the measured data points, solid line – fit, yellow and red lines show the skew-gaussian components. (For interpretation of the references to colour in this figure legend, the reader is referred to the web version of this article.)

Q_y absorption (minus the vibronic bands). This is equivalent to ~ 10 Chls, assuming that the complex contains 143 Chl a and 12 Chl b . Subtracting two RC Chls, which should absorb at ~ 702 nm [57,58], and further assuming that the absorption at 705 nm, equivalent to three Chls, originates from the core complex, we arrive at a number of 5 red states in LHCI – 3 absorbing at 705–708 nm and 2 at 712 nm. It should be emphasized that the distribution of “states” between two bands with a defined position is somewhat arbitrary as the absorption is spread over a broad range of wavelengths extending beyond 720 nm.

3.1.2. Fluorescence emission spectra

The fluorescence emission spectra of the PSI core and the PSI-LHCI supercomplex recorded at 77 K and their gaussian decomposition are plotted in Fig. 2. The emission spectra have pronounced peaks at 720 and 733 nm, for the isolated core and the intact supercomplex, respectively. In both sample types, low-intensity emission bands below 700 nm are visible, representing emission from the bulk antenna Chls. Following the mirror-image rule, the spectra are decomposed into asymmetric gaussians skewed toward longer wavelengths. The main emission band of the PSI core was decomposed into two main components at 714 and 721 nm and two low-intensity bands at 705, 733 nm. The main emission of intact PSI-LHCI was described by bands at 714, 724, 732 and 743 nm and a broad component around 760 nm, probably of vibronic nature.

3.2. Fluorescence kinetics

3.2.1. Global lifetime analysis

To follow the dynamics of excitation equilibration with the red Chls, we recorded the fluorescence decay kinetics at temperature of 77 K using 440-nm excitation pulses. Note that room-temperature fluorescence kinetics of the same samples have been previously published [30]. The kinetics over a 10-ns time period, for both the isolated core

and the intact PSI-LHCI, could be described satisfactorily with six exponential decay terms obtained by global analysis. The resultant decay-associated emission spectra (DAES) are shown in Fig. 3 and the contribution of each component (the relative DAES area) are listed in Supplementary Table S3. The measured fluorescence kinetics and the DAES data are available online [59].

In the core complex (Fig. 3a), the shortest lifetime of 19 ps dominates the fluorescence decay at 680–690 nm while emission at longer wavelengths rises with this lifetime, as shown by the negative amplitude of the DAES. The markedly nonconservative shape of the DAES suggests loss of excitations occurring on this timescale in addition to transfer to the long-wavelength forms. The fluorescence above 700 nm decays with three main lifetimes – 79 ps, 340 ps and 1 ns, characterized by positively-signed, broad DAES with maxima around 705, 715 and 720 nm, respectively. The two longest-lived components (2.6 and 5.8 ns), with $\sim 2\%$ contribution each, are due to minor impurities in the sample. The 2.6-ns component represents free LHCI as it has a similar DAES as the 2.8-ns component in PSI-LHCI (Fig. 3b) and amplitude corresponding to the amount of Lhca contamination in the core sample (see Section 2.1). The blue-shifted spectrum of the longest component, peaking at 675 nm, clearly associates it with free Chls.

In the PSI-LHCI supercomplex (Fig. 3b), the fastest fluorescence decay component (16 ps) is characterized by a DAES with a positive maximum at 690 nm and a negative one at about 730 nm. A negative shoulder is also noticeable around 715 nm. Evidently, this component represents not only trapping and equilibration of excitations in the core but also equilibration with red Chls in LHCI (at 730 nm). The second component, with a lifetime of 64 ps, shows decay of states emitting around 705 nm and corresponding rise of emission at 730–735 nm. Both the 16 and 64 ps components have larger area above the zero line, indicating excitation trapping in addition to equilibration. At least three longer-lived components characterize the fluorescence decay in the far-red region whose positive-only DAES show maxima at 715, 722 and

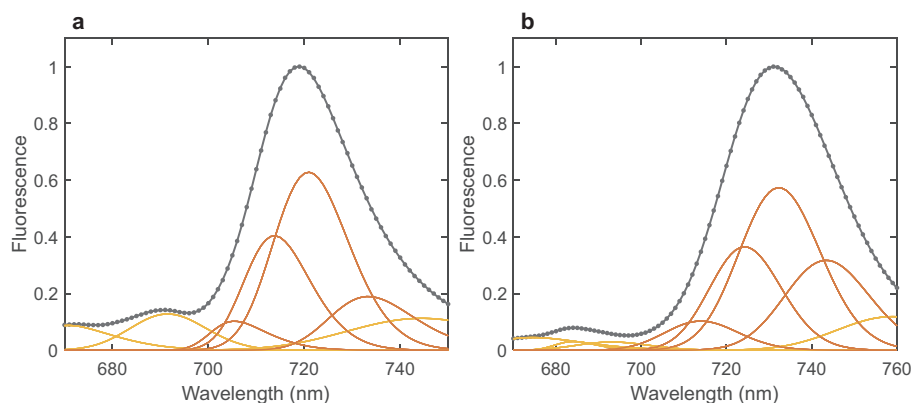


Fig. 2. Gaussian decomposition analysis of the fluorescence emission spectra of PSI at 77 K. (a) PSI core complex; (b) PSI-LHCI supercomplex. Gray symbols indicate the measured data points, solid line – fit, yellow and red lines show the skew-gaussian components. (For interpretation of the references to colour in this figure legend, the reader is referred to the web version of this article.)

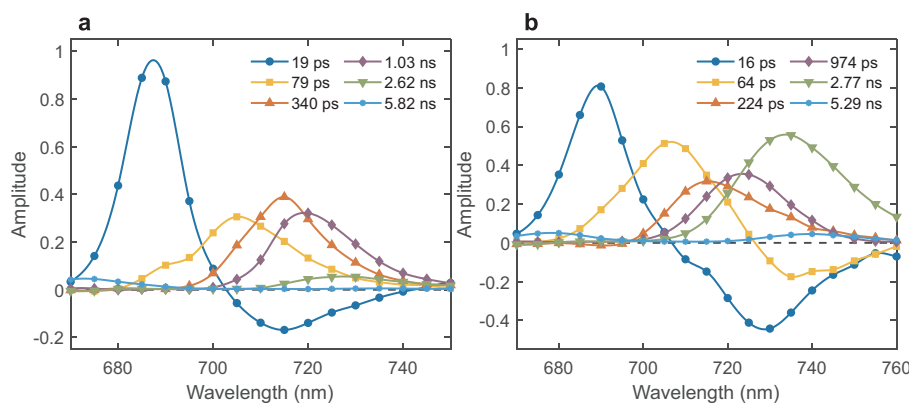


Fig. 3. Decay-associated fluorescence emission spectra of isolated PSI complexes obtained from global analysis of the fluorescence decays measured by TCSPC. (a) PSI core complex; (b) intact PSI-LHCI supercomplex. The corresponding lifetimes are as indicated. Note that the amplitudes of the first DAES (16, 19 ps) are divided by 2.

733 nm. The first two are very similar to the 340-ps and 1-ns components resolved in the isolated core. Finally, the longest lifetime (5.3 ns) with a 3% total contribution shows decay of a small population of free Chls (at 675 nm) as well as red-shifted forms (740 nm).

The drastic slowdown of the fluorescence decay at longer wavelengths is well illustrated by the wavelength dependence of the average lifetime, as a proxy of the exciton trapping time (Fig. 4). Interestingly, the average lifetime is almost equal at 680–700 nm for both the isolated core and the intact supercomplex – around 20 ps. The fluorescence lifetime at 740 nm is about two orders of magnitude slower, showing that photochemical trapping of excitations on the red Chls is ineffectual at 77 K in both complexes.

3.2.2. Spectral decomposition of the time-resolved fluorescence

The red spectral forms in the core and the peripheral antenna were additionally examined by global fitting of asymmetric gaussian bands to the time-resolved emission spectra (TRES) in a time window from 10 ps to 2 ns. Fits of the TRES reconstructed from the DAES are shown in Fig. 5. The TRES show the rapid decay of fluorescence at 680–690 nm that is followed by a slow decay of the far-red emission accompanied by gradual red shift as energy is transferred to the red Chls. We point out that in PSI-LHCI (Fig. 5b), the maximal fluorescence at 735 nm is not reached until ~100 ps.

Five skew-gaussian bands were necessary to fit the TRES of the isolated core – with maxima at 674, 688, 705, 715, 722 nm, plus an additional broad band at 742 nm. It is notable that the peaks coincide

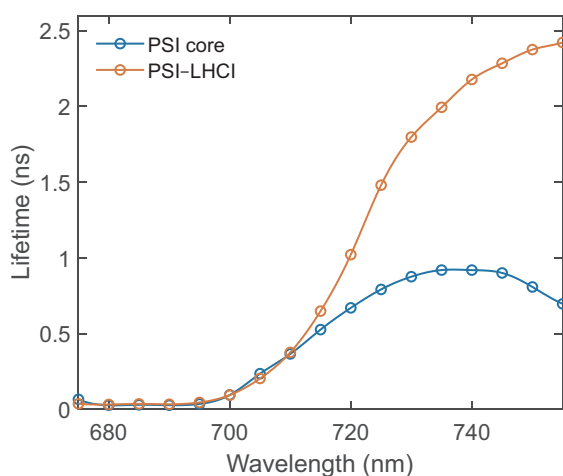


Fig. 4. Wavelength dependence of the amplitude-weighted average fluorescence lifetime $\tau_{av} = \sum_i a_i \tau_i / \sum_i a_i$ for the PSI core and PSI-LHCI at 77 K. Note that decay component with ~5-ns lifetime attributed to free Chls are excluded from the calculation.

with the maxima of the DAES. This is a strong indication that the species emitting at 715 and 722 nm decay independently. For PSI-LHCI, the TRES could be approximated with six components, whose peak positions, also in this case, closely matched the DAES – 679, 690, 704, 714, 722, 735 nm, and an additional one at 755 nm. The spectral decomposition of the TRES for several selected times is plotted in Supplementary Fig. S2. The time-dependent amplitudes of the spectral components (Supplementary Fig. S3) show that the states emitting around 705 and 715 nm have substantial population already at 10 ps, indicating that spectral equilibration has occurred on timescale faster than the experiment time resolution.

3.2.3. Dynamics of spectral evolution

A useful parameter related to the dynamic energy redistribution in the antenna is the time-dependent first spectral moment of the TRES, which is a measure of the mean energy of the emitting chromophores [23,38]:

$$S_1(t) = \int \nu F(\nu; t) d\nu,$$

where ν is frequency (wavenumber) and $F(\nu; t)$ is the TRES at time t . We used the DAES to calculate the spectral moment for the isolated PSI core and the intact PSI-LHCI supercomplex (Fig. 6) – which allows us to discard the emission from free Chls. The spectral moment provides no new information per se, but a simple representation of the spectral evolution (time-dependent energy shift). The core complex dynamics can be described with two exponential lifetimes. The fast one, ~30 ps, is responsible for 85% of the spectral evolution and represents the shift from bulk Chls to red forms. The slower component, ~400 ps, represents equilibration processes between the red forms, particularly those emitting near 720 nm. For PSI-LHCI, the spectral moment shows somewhat slower dynamics, with lifetimes of 17, 72 and 660 ps (Fig. 6), owing to the slower equilibration with red states in LHCI.

From these data, we can extract the mean characteristic time of spectral evolution [38]:

$$\bar{\tau}_{S_1} = \frac{\sum_i a_i \tau_i^2}{\sum_i a_i \tau_i}$$

We obtained timescales of 312 ps and 496 ps for the core and supercomplex, respectively. These values are comparable to the reported spectral evolution timescale of 291 ps for PSI-200 particles at 170 K [38].

3.2.4. Kinetic modelling

For further insight into the energy equilibration dynamics, aiming to reveal the pathways of energy equilibration and the corresponding rates, we performed compartmental kinetic modelling (target analysis) of the time-resolved fluorescence data. We tested kinetic model schemes where the number of species was equal to the number of

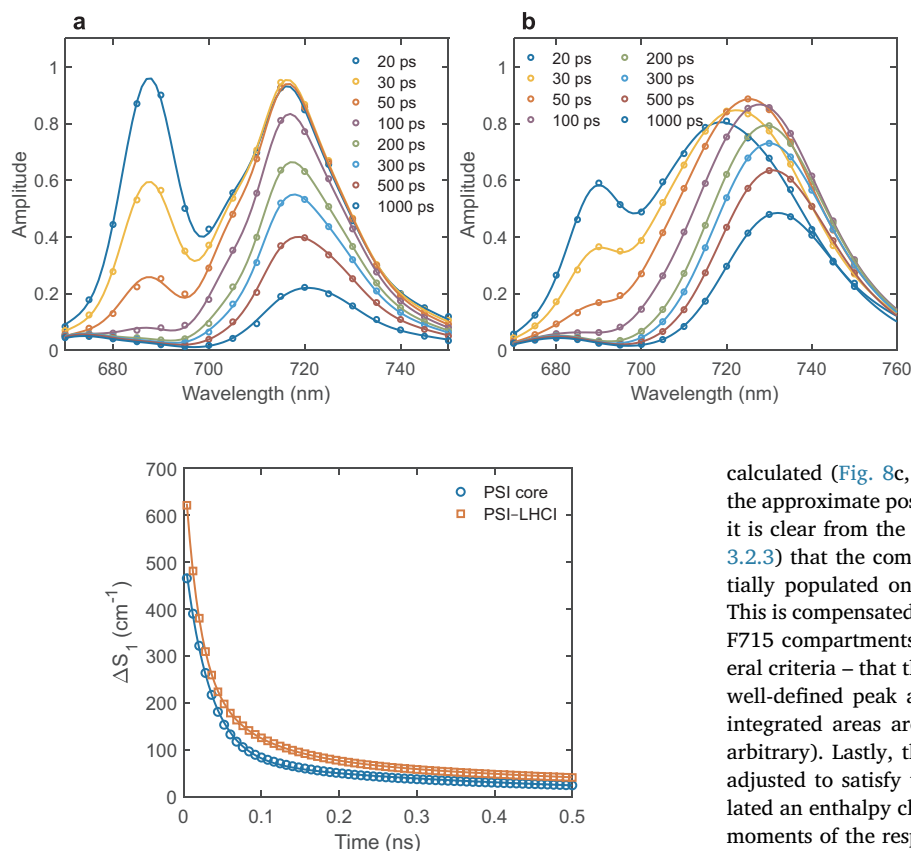


Fig. 6. Time dependence of the mean emission frequency (the first spectral moment of the TRES) for the PSI core complex and PSI-LHCI. Solid lines represent exponential fits of the spectral evolution. See Section 3.2.3 for details.

lifetime components resolved by global analysis, i.e. four in the PSI core and five for PSI-LHCI with additional unconnected components, representing uncoupled LHCI (in the core complex samples) and free pigments. The simplest kinetic scheme – a sequential unbranched irreversible scheme – does not explain well the core complex kinetics (not shown) because it results in broad multimodal species-associated emission spectra (SAES). The spectral decomposition of the TRES indicated that the far-red-emitting components are not connected via direct EET. This leads to a star-shaped connectivity scheme, with an initially excited “bulk” pigment pool equilibrating with “red” compartments (Fig. 7). The models result in decay lifetimes and DAES identical to those obtained by global analysis (Fig. 3); while the compartments are represented by SAES shown in Fig. 8. The species amplitudes and kinetics can be found in Supplementary Table S4 and Fig. S4, respectively. From the amplitudes and decay lifetimes, the species contributions to the stationary fluorescence emission spectrum can be

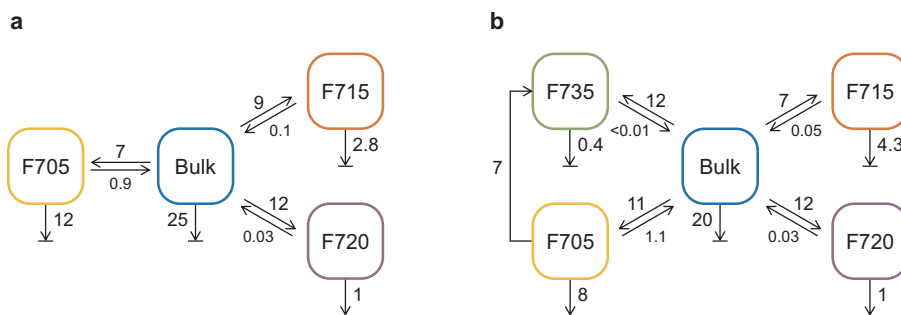


Fig. 7. Kinetic schemes used for target analysis of the fluorescence kinetics and resulting rate constants of energy transfer and trapping (in ns^{-1}). (a) PSI core complex; (b) PSI-LHCI supercomplex. See Section 3.2.4 for details.

Fig. 5. Time-resolved emission spectra (TRES) at selected times reconstructed from the DAES and fitted spectra from gaussian decomposition analysis. (a) PSI core complex; (b) intact PSI-LHCI supercomplex. Symbols and solid lines indicate the TRES and the fitted spectra, respectively. Gaussian components for selected TRES are plotted in Supplementary Fig. S2.

calculated (Fig. 8c, d). The “red” compartments are labeled based on the approximate position of the fluorescence emission maxima. Further, it is clear from the DAES and TRES spectral moment analysis (Section 3.2.3) that the components emitting around 705 and 715 nm are partially populated on timescales faster than the experiment resolution. This is compensated by adding direct excitation (6–9%) to the F705 and F715 compartments. The rate constants are constrained to satisfy several criteria – that the fitted SAES are positive-only, they have only one well-defined peak and approximately skew-gaussian shape, and their integrated areas are comparable (though this condition is somewhat arbitrary). Lastly, the ratio of the forward and backward EET rates is adjusted to satisfy the detailed balance condition. For this, we calculated an enthalpy change from the difference between the first spectral moments of the respective SAES and an entropy change assuming that the core complex contains a total of 98 pigments, and the red compartments are equivalent to 1–2 Chls each.

In the core complex, the 19 ps decay lifetime of the Bulk compartment is determined by both the rate constants of equilibration and excitation loss (trapping) and population of all red forms on the same timescale. The 79-ps decay lifetime is primarily determined by trapping of excitations at F705. The observed 340-ps decay lifetime is due to both decay and equilibration of F715 and the longest lifetime of 1 ns represents the decay of the F720 states. The model of the intact PSI-LHCI, includes one more compartment, F735, which evidently represents red Chls in the peripheral antenna (Fig. 7b). Excluding F735, the scheme is identical to the core complex model and results in similar spectra, only they are red-shifted by 1–3 nm, Bulk has a noticeable shoulder around 715 nm, and F715 has a long-wavelength tail suggesting some mixing with F735. The rates of equilibration and decay are also comparable to the core complex. The F705 compartment, however, is connected to F735 with a rate of 7 ns^{-1} . The connection is demanded by the negative peak of the 64-ps DAES at 735 nm.

We must stress that the kinetic models severely oversimplify the system, which inherently contains more pigment groups and timescales of energy and electron transfer than the five decay components that can

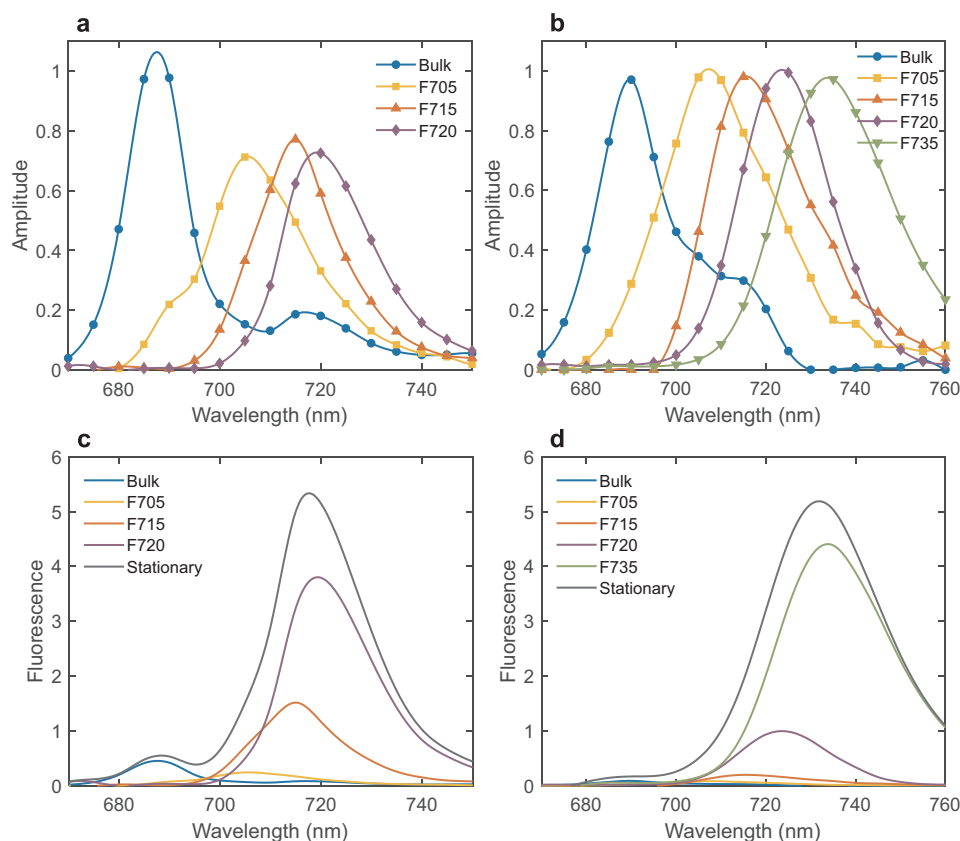


Fig. 8. Species-associated emission spectra resulting from target analysis of the fluorescence kinetics. (a,c) PSI core complex; (b,d) PSI-LHCI supercomplex. In (c) and (d), the spectra are scaled to show their respective contribution to the stationary fluorescence emission spectrum.

be resolved. Clearly, some of the model compartments represent heterogeneous pigment pools, especially the Bulk compartments. We can safely assume that equilibration between the bulk Chls in the core antenna is much faster than EET to the red Chls; however, the same assumption may not be valid in PSI-LHCI. Therefore, the model rate constants, especially in PSI-LHCI, should not be taken as microscopic physical rate constants between physical pigment pools. Furthermore, the rate of excitation trapping, represented as the decay of the Bulk compartment, cannot be accurately determined without a priori knowledge of the exact ratio of the bulk and red Chl emission intensities. Similarly, the branching of EET to the red Chls is fixed by assuming that the oscillator strength of the respective states is identical, which may not be accurate. Finally, the actual forward-to-backward EET ratio to the red-most states can be up to an order of magnitude larger than calculated, because of the large Stokes shifts, which slightly affects the decay rate constants from these states. Thus, while the kinetic models are useful to illustrate the system topology and assign the spectral components, quantitative predictions based on the best-fit rate constants must be made with caution.

In summary, the target analysis suggests that the F715 and F720 compartments represent red Chls in the core antenna, F735 in LHCI, and F705 is contributed by both the core complex and the peripheral antenna.

4. Discussion

4.1. Long-wavelength absorbing and emitting states

By comparing the steady-state absorption and fluorescence emission spectra of the isolated core and the native PSI-LHCI supercomplex, we can distinguish red Chl forms in the two main structural units of plant PSI. Taken separately, the results are in good agreement with published

data. Analyzed together, the different spectroscopic signatures obtained from the same samples and conditions allow us to ascribe the red Chl content with higher confidence. Spectral decomposition of the PSI core absorption revealed a broad band centred at 705 nm. This is well in line with the observed red Chl absorption maxima at 705 to 708 nm in the PSI core of Arabidopsis or maize [9,14]. The band has an oscillator strength equivalent to three Chls – the same number was estimated by Gobets et al. [14] for the PSI core complex from maize. Additional red absorption bands were found in the PSI-LHCI supercomplex at 703 and 712 nm – consistent with the red spectral forms in isolated native and recombinant LHCI complexes – at 704–707 and 709–712 nm [20,60,61]. The red-most band of PSI-200 particles was also found by site-selective fluorescence to be at 712 nm [9] and at 716 nm [62]. The contribution of the core complex to the far-red absorption of the intact PSI-LHCI is ~35% – close to the value of 40%, determined using hole-burning spectroscopy [9]. For LHCI we estimated a total oscillator strength of five Chls. The same value was reported for the far-red absorption of LHCI from maize [14]. Still, we cannot rule out the possibility that some of the additional red absorption in the supercomplex is by red-shifted states in the core or at the interface between the core and peripheral antenna complexes, which may be lost in isolation of the core [5].

The absorption analysis strongly suggests the existence of several antenna Chls in the plant PSI core complex absorbing at wavelengths longer than the RC. In light of the now available high-resolution crystal structures of PSI from plants and the cyanobacteria and their very high degree of similarity, including the position and orientation of antenna Chls, this result is not too surprising. We also analyzed the 77-K absorption spectra of trimeric PSI from the *Synechocystis* PCC6803 and obtained an integrated area of the red bands corresponding to 4.5 Chls – again matching the 4–5 Chls reported by other authors [14,63,64], further corroborating the validity of our quantification.

Although the absorption spectra suggest multiple red states in the core complex, based on the total oscillator strength, different spectral forms cannot be distinguished in the broad structureless far-red absorption band. Contrary to this, three well-separated spectral forms, with maxima around 705, 715 and 722 nm, were clearly distinguished in the fluorescence emission spectra. These bands were not only found by gaussian decomposition of both the steady-state and time-resolved emission spectra, but also appear as separate DAES and SAES in the fluorescence kinetics of the PSI core. Because of its short decay lifetime, the 705-nm component weakly contributes to the steady-state emission spectrum (Fig. 2), which peaks at 720 nm as shown previously [9,14].

It is well-documented that the red-most emission from plant PSI, at 733–735 nm, is due to red states in the peripheral antenna [52,65], located in the subunits Lhca3 and Lhca4 [17,60]. Accordingly, an intense band at 733–735 nm was resolved in all emission spectra of the supercomplex (stationary, TRES, DAES and SAES). It should be mentioned that fluorescence components with maxima at 720 and 735 nm with similar decay lifetimes as reported here (1 and 2.5 ns, respectively) were resolved in PSI-200 particles at 77 K by Mukerji and Sauer (1988) and assigned to the core and peripheral antenna, respectively, based on their excitation-wavelength dependence. Further, a less prominent band centred at 743 nm was also resolved in the stationary spectra (Fig. 2b) and in the longest-lived fluorescence decay component (Fig. 3b). From the DAES amplitude, it can be said that these red-shifted states are in extremely low abundance, although they have a non-negligible contribution to the fluorescence intensity (because of a long decay lifetime). The 732 and 740 nm emission was suggested to originate from the same set of inhomogeneously broadened spectral bands [60].

An additional state in LHCI emitting around 705 nm can be inferred from the fact that 705-nm DAES in PSI-LHCI has a larger amplitude than the corresponding DAES in the core (Fig. 3). Accordingly, the EET rate constant from the Bulk compartment to F705 is higher in PSI-LHCI (Fig. 7b). Gobets and van Grondelle [14] resolved two red pools in the 4 K emission spectra of LHCI – emitting at 702 nm and 733 nm, with absorption at 692 and 711 nm, respectively. We note that a 692-nm absorption band is also present in our gaussian decomposition analysis of PSI-LHCI (Supplementary Table S2).

4.2. Excitation transfer and trapping dynamics

4.2.1. Timescales of spectral equilibration and trapping

Under cryogenic conditions, as the same sample volume is repeatedly excited, the RC can become closed (oxidized), especially if the rate of excitation exceeds the rate of charge recombination. It has been reported that in about 40% of the RCs electron transfer is limited to phyloquinone (A_1) with the $P_{700}^+A_1^-$ radical pair recombining in 0.5 ms [58,66–68]. This is comparable to the excitation rate in our experiments (see Section 2.4). The remaining population of PSI RCs form long-lived charge separated states, where P_{700} will be permanently oxidized during the measurement. This apparent heterogeneity, however, does not radically change the rate of trapping of bulk Chl excitations [69]. The EET dynamics of PSI is also affected at low temperatures [44,48,49,58,70] with the main effect being trapping of excitations on the red Chls, as the available vibrational energy is insufficient for uphill EET back to the bulk antenna [71]. Croce et al. [38] analyzed the energy equilibration processes in PSI-200 by calculating the mean emission frequency from the TRES. They showed that the average timescale of equilibration slowed down from 86 ps at room temperature to 291 ps at 170 K – in both cases of similar magnitude as the timescale of the excitation trapping. Following the same approach, we estimated an average timescale of about 500 ps at 77 K. The slow equilibration was accompanied by dramatic slowdown of the fluorescence decay in the far-red region – in both the isolated core (~1 ns) and the intact supercomplex (~2.5 ns). In contrast, faster decay and comparatively mild wavelength and temperature dependence of the

fluorescence lifetime is observed in the PSI core from *Chlamydomonas*, which does not contain long-wavelength Chls [72]. Thus, red Chls in the higher-plant PSI core efficiently trap bulk excitations, which is the reason for the high fluorescence yield in the far-red region. Because uphill transfer from the red-most states is largely blocked at 77 K, they decay with nanosecond lifetimes, as isolated antenna complexes [65]. Even at physiological temperatures, uphill transfer from the red states slows down the effective trapping in PSI-LHCI by a factor equal or greater than the slowing due to increased antenna size [27,40,73].

4.2.2. Kinetics of the red-emitting states

As discussed in the previous section, the main red-emitting components in the core are at wavelengths of 715 and 720 nm, whereas red states in LHCI emit mostly at 733 nm. In support of this, we find that the corresponding DAES have comparable shapes and amplitudes in both the isolated core and PSI-LHCI. It is tempting to assign the state emitting at 705 nm to the RC pigments – following the gaussian decomposition of the absorption spectrum. In this case, however, the effective trapping time would be too long – 80 ps. Low-temperature studies on PSI from cyanobacteria and green algae have shown that the photochemical trapping time at cryogenic temperatures is comparable to room temperature – 15–20 ps [48,49]. It is then reasonable to assign the 705-nm emission to red-shifted antenna Chls as well. Thus, it would appear that there are three spectrally and kinetically distinct red forms in the core complex, F705, F715 and F720, acting as (pseudo)traps for excitations at 77 K.

The fluorescence kinetics shows that the more red-shifted forms decay with longer lifetimes. Such relationship suggests dynamic downhill equilibration among them, which should be reflected by the DAES having positive and negative peaks – in qualitative disagreement with the experimental data. Sequential relaxation producing all-positive DAES is also possible if the donor states have higher emission at the wavelengths of the acceptor states [38]. However, any tested kinetic model with sequential EET between the red states resulted in unrealistically broad and bimodal SAES. Therefore, we conclude that all red forms in the core decay almost independently at 77 K, some equilibration with the bulk antenna notwithstanding. The lack of connectivity between the red states has been discussed in several works [23,27,38,74] – it has been hypothesized that the different forms reflect structural heterogeneity of PSI rather than different Chl sites. If the three species decay mostly independently though, there must be a reasonable explanation for the short decay lifetimes, particularly of F705 and F715.

As pointed out already, a fraction of RCs are inevitably in an oxidized state under the conditions for measuring the fluorescence kinetics at 77 K. The rate constants of decay of the Bulk compartments in the kinetic models (Fig. 7) therefore represent average time constants of this heterogeneous trapping. The oxidized RC (P_{700}^+) itself is an efficient quencher of Chl singlet excited states [75]. Due to its broad absorption extending into the far-red region, the cation radical can accept energy both from the bulk and red-shifted Chls and the excited P_{700}^{+*} rapidly decays via internal conversion [58]. The decay lifetimes of F705 and F715 could then be mainly determined by the rates of Förster energy transfer to P_{700}^+ , which in turn depends on the spectral overlap and the relative distance and orientation of the transition dipoles [76]. Another possible mechanism of quenching is by charge separation, and subsequent recombination. Giera et al. [77] proposed that the positive charge on P_{700}^+ facilitates fast charge recombination between the RC Chls A^+ and A_0^- , with an apparent lifetime of 25 ps (in *Chlamydomonas*). Recently, the fluorescence decay kinetics of plant PSI with preoxidized P_{700} has been explained by a similar mechanism [69]. At room temperature, recombination of the alternative radical pair formed in the closed RCs can repopulate the excited RC and result in emission from P_{700}^* ; however, at 77 K radiationless recombination to the ground-state RC may prevail. For either mechanism we have to assume that the F705, F715 and F720 states have progressively weaker coupling to P_{700} .

Regardless of the mechanism of decay of the red Chls, we can estimate from the kinetic model of the core complex (Fig. 7) that 42% of the bulk antenna excitations are trapped in the RC (expressed as the decay of the Bulk compartment) – about the same number (50%) was reported for *Synechococcus elongatus* [71]. The remaining excitations are trapped by the red Chls. Interestingly, all red forms have comparable contribution to trapping excitations on bulk antenna Chls at 77 K, as shown by the rate constants of EET (Fig. 7). However, mainly because of their different decay lifetimes, the red Chls contribute differently to the stationary fluorescence intensity (Fig. 8c, d).

In contrast to the isolated core, we resolved two rise times of the red-emitting states in PSI-LHCI (Fig. 3). The faster timescale (16 ps) is comparable to the main decay lifetime of bulk antenna excitations in the core, but the DAES shows additional negative amplitude at 730–735 nm. Therefore, bulk-red equilibration also occurs on this timescale in LHCI – similar equilibration times are observed in isolated LHCI and PSI-LHCI at room temperature [29]. The second component (64 ps) clearly shows downhill transfer from F705 to F735. Thus, F705 compartment in PSI-LHCI includes additional red forms in the peripheral antenna, as discussed above.

5. Conclusions

The higher-plant PSI core complex investigated here, similar to PSI from cyanobacteria, contains multiple long-wavelength Chl forms. We confirm some earlier estimations that red forms absorbing at wavelengths around 705 nm carry a total oscillator strength of at least three Chls. Three spectrally and kinetically distinct spectral forms emitting at wavelengths near 705, 715 and 722 nm were resolved. A kinetic model of the picosecond time-resolved fluorescence at 77 K is in agreement with a view that the red Chls are dispersed in the core antenna and not directly coupled to each other via EET. In contrast, Chls emitting around 705 nm in LHCI transfer to the red-most forms at 735 nm on a timescale of ~60 ps. According to the model, ~40% of the bulk antenna excitations in the isolated core are directly trapped by the RC, whereas the rest decay non-photochemically via the red Chls. From these results it becomes apparent that the red antenna Chls in the core complex must not be neglected when interpreting kinetic experimental results. Recent models of the dynamics of EET and charge separation in plant PSI [30,51,69] may need to be extended to incorporate this information.

Author contributions

PL and PA designed and performed the experiments, analyzed the data and wrote the manuscript.

Declaration of competing interest

The authors declare that they have no known competing financial interests or personal relationships that could have appeared to influence the work reported in this paper.

Acknowledgements

The work was supported by grants from the Hungarian Ministry for National Economy (GINOP-2.3.2-15-2016-00001) and the National Research, Development and Innovation Fund NKFI NN-124904, 2018-1.2.1-NKP-2018-00009. We are grateful to Mira Sass for the help with sample preparation and Avratanu Biswas for partaking in the kinetic analysis. We thank Dr. Bettina Ughy for her help with protein composition analysis.

Research data

The data (absorption, steady-state and time-resolved fluorescence

spectra) presented in this article are available for download online [59].

Appendix A. Supplementary data

Supplementary data to this article can be found online at <https://doi.org/10.1016/j.bbabi.2020.148274>.

References

- [1] P. Fromme, P. Jordan, N. Krauß, Structure of photosystem I, *Biochim. Biophys. Acta* 1507 (2001) 5–31.
- [2] J.H. Golbeck, The binding of cofactors to photosystem I analyzed by spectroscopic and mutagenic methods, *Annu. Rev. Biophys. Biomol. Struct.* 32 (2003) 237–256.
- [3] N. Nelson, W. Junge, Structure and energy transfer in photosystems of oxygenic photosynthesis, *Annu. Rev. Biochem.* 84 (2015) 659–683.
- [4] X.C. Qin, M. Suga, T.Y. Kuang, J.R. Shen, Structural basis for energy transfer pathways in the plant PSI-LHCI supercomplex, *Science* 348 (2015) 989–995.
- [5] Y. Mazar, A. Borovikova, N. Nelson, The structure of plant photosystem I supercomplex at 2.8 Å resolution, *eLife*, 4 (2015) e7433.
- [6] R. Nagao, K. Kato, K. Ifuku, T. Suzuki, M. Kumazawa, I. Uchiyama, Y. Kashino, N. Dohmae, S. Akimoto, J.-R. Shen, Structural basis for assembly and function of a diatom photosystem I-light-harvesting supercomplex, *Nat. Commun.* 11 (2020) 1–12.
- [7] N. Nelson, A. Ben-Shem, The complex architecture of oxygenic photosynthesis, *Nat. Rev. Mol. Cell Biol.* 5 (2004) 971–982.
- [8] N.V. Karapetyan, E. Schlodder, R. van Grondelle, J.P. Dekker, The long-wavelength chlorophylls of photosystem I, in: J.H. Golbeck (Ed.), *Photosystem I: The Light-driven, Plastocyanin: Ferredoxin Oxidoreductase*, Springer, Dordrecht, The Netherlands, 2006, pp. 177–192.
- [9] J.A. Ihalainen, M. Rätsep, P.E. Jensen, H.V. Scheller, R. Croce, R. Bassi, J.E. Korppi-Tommola, A. Freiberg, Red spectral forms of chlorophylls in green plant PSI: a site-selective and high-pressure spectroscopy study, *J. Phys. Chem. B* 107 (2003) 9086–9093.
- [10] E. Romero, M. Mozzo, I.H. Van Stokkum, J.P. Dekker, R. Van Grondelle, R. Croce, The origin of the low-energy form of photosystem I light-harvesting complex Lhca4: mixing of the lowest exciton with a charge-transfer state, *Biophys. J.* 96 (2009) L35–L37.
- [11] V.I. Novoderezhkin, R. Croce, M. Wahadoszamen, I. Polukhina, E. Romero, R. van Grondelle, Mixing of exciton and charge-transfer states in light-harvesting complex Lhca4, *Phys. Chem. Chem. Phys.* 18 (2016) 19368–19377.
- [12] S. Vaitekoniis, G. Trinkunas, L. Valkunas, Red chlorophylls in the exciton model of photosystem I, *Photosynth. Res.* 86 (2005) 185–201.
- [13] R.N. Frese, M.A. Palacios, A. Azzizi, I.H. Van Stokkum, J. Kruip, M. Rögner, N.V. Karapetyan, E. Schlodder, R. van Grondelle, J.P. Dekker, Electric field effects on red chlorophylls, β -carotenes and P700 in cyanobacterial photosystem I complexes, *Biochim. Biophys. Acta* 1554 (2002) 180–191.
- [14] B. Gobets, R. van Grondelle, Energy transfer and trapping in photosystem I, *Biochim. Biophys. Acta* 1507 (2001) 80–99.
- [15] N.V. Karapetyan, D. Dorra, G. Schweitzer, I.N. Bezmertnaya, A.R. Holzwarth, Fluorescence spectroscopy of the longwave chlorophylls in trimeric and monomeric photosystem I core complexes from the cyanobacterium *Spirulina platensis*, *Biochemistry* 36 (1997) 13830–13837.
- [16] R. Croce, G. Zucchelli, F.M. Garlaschi, R. Bassi, R.C. Jennings, Excited state equilibration in the photosystem I – light-harvesting I complex: P700 is almost isoenergetic with its antenna, *Biochemistry* 35 (1996) 8572–8579.
- [17] R. Croce, G. Zucchelli, F.M. Garlaschi, R.C. Jennings, A thermal broadening study of the antenna chlorophylls in PSI-200, LHCI, and PSI core, *Biochemistry* 37 (1998) 17355–17360.
- [18] V.H. Schmid, K.V. Cammarata, B.U. Bruns, G.W. Schmidt, *In vitro* reconstitution of the photosystem I light-harvesting complex LHCI-730: heterodimerization is required for antenna pigment organization, *Proc. Natl. Acad. Sci. U. S. A.* 94 (1997) 7667–7672.
- [19] S. Castelletti, T. Morosinotto, B. Robert, S. Caffarri, R. Bassi, R. Croce, Recombinant Lhca2 and Lhca3 subunits of the photosystem I antenna system, *Biochemistry* 42 (2003) 4226–4234.
- [20] R. Croce, A. Chojnicka, T. Morosinotto, J.A. Ihalainen, F. Van Mourik, J.P. Dekker, R. Bassi, R. Van Grondelle, The low-energy forms of photosystem I light-harvesting complexes: spectroscopic properties and pigment-pigment interaction characteristics, *Biophys. J.* 93 (2007) 2418–2428.
- [21] R. Croce, H. van Amerongen, Light-harvesting in photosystem I, *Photosynth. Res.* 116 (2013) 1–14.
- [22] W. Butler, C. Tredwell, R. Malkin, J. Barber, The relationship between the lifetime and yield of the 735 nm fluorescence of chloroplasts at low temperatures, *Biochim. Biophys. Acta* 545 (1979) 309–315.
- [23] R.C. Jennings, G. Zucchelli, R. Croce, F.M. Garlaschi, The photochemical trapping rate from red spectral states in PSI-LHCI is determined by thermal activation of energy transfer to bulk chlorophylls, *Biochim. Biophys. Acta* 1557 (2003) 91–98.
- [24] V. Paschenko, S. Protasov, A. Rubin, K. Timofeev, L. Zamazova, L. Rubin, Probing the kinetics of photosystem I and photosystem II fluorescence in pea chloroplasts on a picosecond pulse fluorometer, *Biochim. Biophys. Acta* 408 (1975) 143–153.
- [25] G. Beddard, G. Porter, C. Tredwell, J. Barber, Fluorescence lifetimes in the photosynthetic unit, *Nature* 258 (1975) 166–168.
- [26] G. Searle, J. Barber, L. Harris, G. Porter, C. Tredwell, Picosecond laser study of

- fluorescence lifetimes in spinach chloroplast photosystem I and photosystem II preparations, *Biochim. Biophys. Acta* 459 (1977) 390–401.
- [27] E. Engelmann, G. Zucchelli, A.P. Casazza, D. Brogioli, F.M. Garlaschi, R.C. Jennings, Influence of the photosystem I-light harvesting complex I antenna domains on fluorescence decay, *Biochemistry* 45 (2006) 6947–6955.
- [28] C. Slavov, M. Ballottari, T. Morosinotto, R. Bassi, A.R. Holzwarth, Trap-limited charge separation kinetics in higher plant photosystem I complexes, *Biophys. J.* 94 (2008) 3601–3612.
- [29] E. Wientjes, I.H. van Stokkum, H. van Amerongen, R. Croce, The role of the individual LhcAs in photosystem I excitation energy trapping, *Biophys. J.* 101 (2011) 745–754.
- [30] P. Akhtar, C. Zhang, Z. Liu, H.S. Tan, P.H. Lambrev, Excitation transfer and trapping kinetics in plant photosystem I probed by two-dimensional electronic spectroscopy, *Photosynth. Res.* 135 (2018) 239–250.
- [31] M.G. Müller, J. Niklas, W. Lubitz, A.R. Holzwarth, Ultrafast transient absorption studies on photosystem I reaction centers from *Chlamydomonas reinhardtii*. 1. A new interpretation of the energy trapping and early electron transfer steps in photosystem I, *Biophys. J.*, 85 (2003) 3899–3922.
- [32] M.G. Müller, C. Slavov, R. Luthra, K.E. Redding, A.R. Holzwarth, Independent initiation of primary electron transfer in the two branches of the photosystem I reaction center, *Proc. Natl. Acad. Sci. U. S. A.* 107 (2010) 4123–4128.
- [33] L. Valkunas, V. Liuolia, J.P. Dekker, R. Grondelle, Description of energy migration and trapping in photosystem I by a model with two distance scaling parameters, *Photosynth. Res.* 43 (1995) 149–154.
- [34] S. Savikhin, W. Xu, P.R. Chitnis, W.S. Struve, Ultrafast primary processes in PS I from *Synechocystis* sp. PCC 6803: roles of P700 and A₀, *Biophys. J.*, 79 (2000) 1573–1586.
- [35] S. Savikhin, W. Xu, P. Martinsson, P.R. Chitnis, W.S. Struve, Kinetics of charge separation and A₀⁻ → A₁ electron transfer in photosystem I reaction centers, *Biochemistry* 40 (2001) 9282–9290.
- [36] D.A. Cherepanov, I.V. Shelaev, F.E. Gostev, A.V. Aybush, M.D. Mamedov, V.A. Shuvalov, A.Y. Semenov, V.A. Nadochenko, Generation of ion-radical chlorophyll states in the light-harvesting antenna and the reaction center of cyanobacterial photosystem I, *Photosynth. Res.* (2020), <https://doi.org/10.1007/s11220-020-00731-0>.
- [37] D.A. Cherepanov, I.V. Shelaev, F.E. Gostev, M.D. Mamedov, A.A. Petrova, A.V. Aybush, V.A. Shuvalov, A.Y. Semenov, V.A. Nadochenko, Mechanism of adiabatic primary electron transfer in photosystem I: femtosecond spectroscopy upon excitation of reaction center in the far-red edge of the Q_Y band, *Biochim. Biophys. Acta* 1858 (2017) 895–905.
- [38] R. Croce, D. Dorra, A.R. Holzwarth, R.C. Jennings, Fluorescence decay and spectral evolution in intact photosystem I of higher plants, *Biochemistry* 39 (2000) 6341–6348.
- [39] J.A. Ihalainen, P.E. Jensen, A. Haldrup, I.H.M. van Stokkum, R. van Grondelle, H.V. Scheller, J.P. Dekker, Pigment organization and energy transfer dynamics in isolated photosystem I (PSI) complexes from *Arabidopsis thaliana* depleted of the PSI-G, PSI-K, PSI-L, or PSI-N subunit, *Biophys. J.* 83 (2002) 2190–2201.
- [40] J.A. Ihalainen, I.H.M. van Stokkum, K. Gibasiewicz, M. Germano, R. van Grondelle, J.P. Dekker, Kinetics of excitation trapping in intact photosystem I of *Chlamydomonas reinhardtii* and *Arabidopsis thaliana*, *Biochim. Biophys. Acta* 1706 (2005) 267–275.
- [41] G. Hastings, L.J. Reed, S. Lin, R.E. Blankenship, Excited state dynamics in photosystem I: effects of detergent and excitation wavelength, *Biophys. J.* 69 (1995) 2044.
- [42] S. Savikhin, W. Xu, V. Soukoulis, P.R. Chitnis, W.S. Struve, Ultrafast primary processes in photosystem I of the cyanobacterium *Synechocystis* sp. PCC 6803, *Biophys. J.*, 76 (1999) 3278–3288.
- [43] E.G. Andrizhivskaya, D. Frolov, R. van Grondelle, J.P. Dekker, Energy transfer and trapping in the photosystem I complex of *Synechococcus* PCC 7942 and in its supercomplex with IsiA, *Biochim. Biophys. Acta* 1656 (2004) 104–113.
- [44] A.N. Melkozernov, S. Lin, R.E. Blankenship, Femtosecond transient spectroscopy and excitonic interactions in photosystem I, *J. Phys. Chem. B* 104 (2000) 1651–1656.
- [45] K. Gibasiewicz, V.M. Ramesh, A.N. Melkozernov, S. Lin, N.W. Woodbury, R.E. Blankenship, A.N. Webber, Excitation dynamics in the core antenna of PS I from *Chlamydomonas reinhardtii* CC 2696 at room temperature, *J. Phys. Chem. B* 105 (2001) 11498–11506.
- [46] K. Gibasiewicz, V. Ramesh, S. Lin, K. Redding, N. Woodbury, A. Webber, Two equilibration pools of chlorophylls in the photosystem I core antenna of *Chlamydomonas reinhardtii*, *Photosynth. Res.* 92 (2007) 55–63.
- [47] A.N. Melkozernov, J. Kargul, S. Lin, J. Barber, R.E. Blankenship, Energy coupling in the PSI-LHCI supercomplex from the green alga *Chlamydomonas reinhardtii*, *J. Phys. Chem. B* 108 (2004) 10547–10555.
- [48] A.N. Melkozernov, J. Kargul, S. Lin, J. Barber, R.E. Blankenship, Spectral and kinetic analysis of the energy coupling in the PS I-LHC I supercomplex from the green alga *Chlamydomonas reinhardtii* at 77 K, *Photosynth. Res.* 86 (2005) 203–216.
- [49] K. Gibasiewicz, V.M. Ramesh, S. Lin, N.W. Woodbury, A.N. Webber, Excitation dynamics in eukaryotic PS I from *Chlamydomonas reinhardtii* CC 2696 at 10 K. Direct detection of the reaction center exciton states, *J. Phys. Chem. B*, 106 (2002) 6322–6330.
- [50] A.R. Holzwarth, M.G. Müller, J. Niklas, W. Lubitz, Charge recombination fluorescence in photosystem I reaction centers from *Chlamydomonas reinhardtii*, *J. Phys. Chem. B* 109 (2005) 5903–5911.
- [51] E. Molotokaitė, W. Remelli, A.P. Casazza, G. Zucchelli, D. Polli, G. Cerullo, S. Santabarbara, Trapping dynamics in photosystem I-light harvesting complex I of higher plants is governed by the competition between excited state diffusion from low energy states and photochemical charge separation, *J. Phys. Chem. B* 121 (2017) 9816–9830.
- [52] I. Mukerji, K. Sauer, Temperature dependent steady state and picosecond kinetic fluorescence measurements of a photosystem I preparation from spinach, in: W.R. Briggs (Ed.), *Photosynthesis, Plant Biology*, Alan R. Liss, New York, 1989, pp. 105–122.
- [53] F.A.L.J. Peters, J.E. van Wielink, H.W. Wong Fong Sang, S. De Vries, R. Kraayenhof, Studies on well coupled photosystem I-enriched subchloroplast vesicles. Content and redox properties of electron-transfer components, *Biochim. Biophys. Acta*, 722 (1983) 460–470.
- [54] P. Akhtar, M. Lingvay, T. Kiss, R. Deák, A. Bóta, B. Ughy, G. Garab, P.H. Lambrev, Excitation energy transfer between light-harvesting complex II and photosystem I in reconstituted membranes, *Biochim. Biophys. Acta* 1857 (2016) 462–472.
- [55] R.J. Porra, W.A. Thompson, P.E. Kriedemann, Determination of accurate extinction coefficients and simultaneous equations for assaying chlorophyll *a* and chlorophyll *b* extracted with 4 different solvents: verification of the concentration of chlorophyll standards by atomic absorption spectroscopy, *Biochim. Biophys. Acta* 975 (1989) 384–394.
- [56] G. Zucchelli, R.C. Jennings, F.M. Garlaschi, The presence of long-wavelength chlorophyll *a* spectral forms in the light-harvesting chlorophyll *a/b* protein complex II, *J. Photochem. Photobiol. B Biol.* 6 (1990) 381–394.
- [57] J.K. Gillie, P.A. Lyle, G.J. Small, J.H. Golbeck, Spectral hole burning of the primary electron donor state of photosystem I, *Photosynth. Res.* 22 (1989) 233–246.
- [58] M. Byrdin, I. Rimke, E. Schlodder, D. Stehlik, T.A. Roelofs, Decay kinetics and quantum yields of fluorescence in photosystem I from *Synechococcus elongatus* with P700 in the reduced and oxidized state: are the kinetics of excited state decay trap-limited or transfer-limited? *Biophys. J.* 79 (2000) 992–1007.
- [59] P. Akhtar, P.H. Lambrev, On the spectral properties and excitation dynamics of long-wavelength chlorophylls in higher-plant Photosystem I, *Mendeley Data* (2020) V1, <https://doi.org/10.17632/kfj5vkr26g.1>.
- [60] J.A. Ihalainen, B. Gobets, K. Sznee, M. Brazzoli, R. Croce, R. Bassi, R. van Grondelle, J.E.I. Korppi-Tommola, J.P. Dekker, Evidence for two spectroscopically different dimers of light-harvesting complex I from green plants, *Biochemistry* 39 (2000) 8625–8631.
- [61] E. Wientjes, R. Croce, The light-harvesting complexes of higher-plant photosystem I: Lhc1/4 and Lhc2/3 form two red-emitting heterodimers, *Biochem. J.* 433 (2011) 477–485.
- [62] B. Gobets, H. van Amerongen, R. Monshouwer, J. Kruij, M. Rögner, R. van Grondelle, J.P. Dekker, Polarized site-selected fluorescence spectroscopy of isolated photosystem I particles, *Biochim. Biophys. Acta* 1188 (1994) 75–85.
- [63] J. Hayes, S. Matsuzaki, M. Rätsep, G. Small, Red chlorophyll *a* antenna states of photosystem I of the cyanobacterium *Synechocystis* sp. PCC 6803, *J. Phys. Chem. B*, 104 (2000) 5625–5633.
- [64] B. Gobets, I.H.M. van Stokkum, M. Rogner, J. Kruij, E. Schlodder, N.V. Karapetyan, J.P. Dekker, R. van Grondelle, Time-resolved fluorescence emission measurements of photosystem I particles of various cyanobacteria: a unified compartmental model, *Biophys. J.* 81 (2001) 407–424.
- [65] I. Mukerji, K. Sauer, Energy transfer dynamics of an isolated light harvesting complex of photosystem I from spinach: time-resolved fluorescence measurements at 295 K and 77 K, *Biochim. Biophys. Acta* 1142 (1993) 311–320.
- [66] E. Schlodder, K. Falkenberg, M. Gergeleit, K. Brettel, Temperature dependence of forward and reverse electron transfer from A₁⁻, the reduced secondary electron acceptor in photosystem I, *Biochemistry* 37 (1998) 9466–9476.
- [67] E. Schlodder, M. Çetin, M. Byrdin, I.V. Terekhova, N.V. Karapetyan, P700⁺ - and ³P700-induced quenching of the fluorescence at 760 nm in trimeric photosystem I complexes from the cyanobacterium *Arthrospira platensis*, *Biochim. Biophys. Acta* 1706 (2005) 53–67.
- [68] G. Milanovsky, O. Gupta, A. Petrova, M. Mamedov, M. Gorka, D. Cherepanov, J.H. Golbeck, A. Semenov, Multiple pathways of charge recombination revealed by the temperature dependence of electron transfer kinetics in cyanobacterial photosystem I, *Biochim. Biophys. Acta* 1860 (2019) 601–610.
- [69] M. Russo, V. Petropoulos, E. Molotokaitė, G. Cerullo, A.P. Casazza, M. Maiuri, S. Santabarbara, Ultrafast excited-state dynamics in land plants photosystem I core and whole supercomplex under oxidised electron donor conditions, *Photosynth. Res.* 144 (2020) 221–233.
- [70] Y. Jia, J.M. Jean, M.M. Werst, C.-K. Chan, G.R. Fleming, Simulations of the temperature dependence of energy transfer in the PSI core antenna, *Biophys. J.* 63 (1992) 259–273.
- [71] L.-O. Pålsson, C. Flemming, B. Gobets, R. van Grondelle, J.P. Dekker, E. Schlodder, Energy transfer and charge separation in photosystem I: P700 oxidation upon selective excitation of the long-wavelength antenna chlorophylls of *Synechococcus elongatus*, *Biophys. J.* 74 (1998) 2611–2622.
- [72] W. Giera, S. Szewczyk, M.D. McConnell, K.E. Redding, R. van Grondelle, K. Gibasiewicz, Uphill energy transfer in photosystem I from *Chlamydomonas reinhardtii*. Time-resolved fluorescence measurements at 77 K, *Photosynth. Res.*, 137 (2018) 321–335.
- [73] W. Giera, S. Szewczyk, M.D. McConnell, J. Snellenburg, K.E. Redding, R. van Grondelle, K. Gibasiewicz, Excitation dynamics in photosystem I from *Chlamydomonas reinhardtii*. Comparative studies of isolated complexes and whole cells, *Biochim. Biophys. Acta*, 1837 (2014) 1756–1768.
- [74] S. Turconi, N. Weber, G. Schweitzer, H. Strotmann, A.R. Holzwarth, Energy transfer and charge separation kinetics in photosystem I. 2. Picosecond fluorescence study of various PS I particles and light-harvesting complex isolated from higher plants, *Biochim. Biophys. Acta*, 1187 (1994) 324–334.
- [75] V. Shubin, I. Bezsmertnaya, N. Karapetyan, Efficient energy transfer from the long-wavelength antenna chlorophylls to P700 in photosystem I complexes from

- Spirulina platensis*, J. Photochem. Photobiol. B Biol. 30 (1995) 153–160.
- [76] Y. Shibata, A. Yamagishi, S. Kawamoto, T. Noji, S. Itoh, Kinetically distinct three red chlorophylls in photosystem I of *Thermosynechococcus elongatus* revealed by femtosecond time-resolved fluorescence spectroscopy at 15 K, J. Phys. Chem. B 114 (2010) 2954–2963.
- [77] W. Giera, V. Ramesh, A.N. Webber, I. van Stokkum, R. van Grondelle, K. Gibasiewicz, Effect of the P₇₀₀ a pre-oxidation and point mutations near A₀ on the reversibility of the primary charge separation in photosystem I from *Chlamydomonas reinhardtii*, Biochim. Biophys. Acta 1797 (2010) 106–112.